

Bifacial and Angular-Resolved Performance Characterization of Ultrathin Cu(In,Ga)Se₂ Solar Cells Including Nanostructures

Tristan Koehler, Yao Gao, and Martina Schmid*

Bifacial solar cells experience growing interest not just for crystalline silicon photovoltaic modules. Thin-film solar cells deposited on a transparent back contact bring inherent semitransparency, making them ideally suited for bifacial applications. Herein, a systematic investigation of bifacial measurement procedures is performed on semitransparent ultrathin Cu(In,Ga)Se₂ (CIGSe) solar cells on transparent conductive oxide, including nanostructures. The measurements are further extended by angular-resolved performance studies. The bifaciality of the samples is determined to be $\approx 80\%$ in current and $\approx 65\%$ in power, and enables the calculation of an equivalent irradiance for solar cell testing under >1 sun front illumination only. The results are compared to bifacial operation, i.e., simultaneous front and rear irradiance, and to the summation of individual front and rear performance measurements up to 1 sun. It is revealed that highly similar results can be obtained for these approaches and that the integration of nanostructures supports device stabilization. Particularly, the higher (75 nm) SiO₂ nanomeshes can enable performance enhancement. Furthermore, the angular-dependent behavior follows the expected trend of reduced illumination intensity according to the cosine of the incident angle. In these findings, the suitability of semitransparent ultrathin CIGSe solar cells for bifacial operation and the benefit of integrated nanostructures is confirmed.

1. Introduction

Bifacial solar cells have already taken over the market share for crystalline silicon photovoltaic modules.^[1] But also for thin-film technologies bifaciality plays an important role. A particular reason lies in the inherent semitransparency of thin-film devices deposited on a transparent back contact, making them ideally suited for bifacial applications. One corresponding example


are bifacial semitransparent ultrathin Cu(In,Ga)Se₂ (BSTUT CIGSe) solar cells with absorber thicknesses below 500 nm and a transparent conductive oxide (TCO) back contact.^[2]

In contrast to the standard test conditions, established for regular current density–voltage (*JV*) measurements of solar cells, only the technical specification DIN IEC/TS 60904-1-2 VDE V 0126-4-1-2:2022-04 exists for bifacial characterization, including however different measurement approaches.^[3] These methods were compared by several groups mostly for c-Si solar cells.^[4–6] Often similar results could be identified for two-sided compared to one-sided measurements with adjusted light intensity. In contrast to these c-Si devices with a similar rear as front efficiency, the performance of thin-film solar cells may significantly differ depending on the direction of illumination and the absorber thickness. A major reason for the drop of rear efficiency is the asymmetry of the structure and hence a potential charge carrier generation further from

the space-charge region when illuminated from the back. When moving from thin-film to ultrathin-film devices, however, the photon absorption and with it the charge-carrier generation can occur closer to the space charge region, benefitting the rear performance. Given these differences, it is important to compare different methods for bifacial measurements also for thin-film devices, which we perform on the example of ultrathin CIGSe solar cells.

To further illustrate the benefit of thickness reduction for bifacial operation, **Figure 1** compares the front and rear performance of CIGSe solar cells on transparent back contact as given in literature. Figure 1a,b depicts the front and rear efficiency— η_{front} and η_{rear} , respectively—as a function of absorber thickness. While η_{front} generally shows the decrease with thickness as expected due to reduced absorption, this is not true for η_{rear} . In contrast, the latter rises (aside from one exception) as the absorber thickness is reduced; this observation is in line with our explanations provided earlier that the absorber thickness reduction benefits the separation of photo-generated carriers in rear-illuminated devices. The ratio of rear over front efficiency, also called bifaciality and defined in detail below, is depicted in Figure 1c. It reveals an increase from ≈ 0.3 for 2500 nm absorber

T. Koehler, Y. Gao, M. Schmid
Faculty of Physics and CENIDE
University of Duisburg-Essen
Forsthausweg 2, Duisburg 47057, Germany
E-mail: martina.schmid@uni-due.de

 The ORCID identification number(s) for the author(s) of this article can be found under <https://doi.org/10.1002/aesr.202400168>.

© 2024 The Author(s). Advanced Energy and Sustainability Research published by Wiley-VCH GmbH. This is an open access article under the terms of the Creative Commons Attribution License, which permits use, distribution and reproduction in any medium, provided the original work is properly cited.

DOI: 10.1002/aesr.202400168

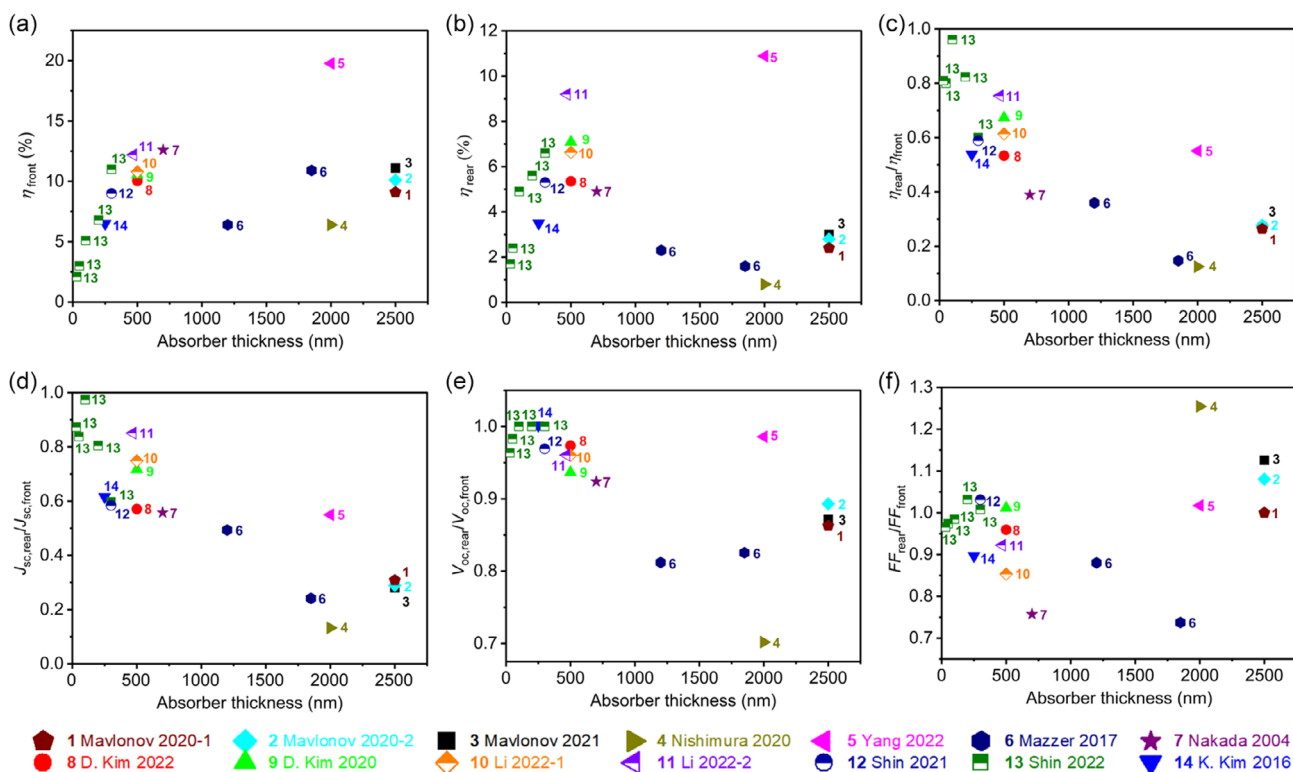


Figure 1. Overview of bifacial performance of CIGSe solar cells on ITO back contact fabricated via a physical vapor deposition (PVD) process: efficiency under a) front illumination η_{front} , b) rear illumination η_{rear} , as well as rear over front ratios of performance parameters, c) efficiency η , d) short-circuit current density J_{sc} , e) open-circuit voltage V_{oc} , and f) fill factor FF ; all values refer to illumination with 1 sun. Data originate from the following references: ref. [4].

thickness to almost 1.0, i.e., comparable front and rear efficiency, for 30 nm. Figure 1d–f gives the ratios of rear over front short-circuit current density (J_{sc}), open-circuit voltage (V_{oc}), and fill factor (FF), respectively. The current ratios essentially reflect the efficiency evolution as a function of absorber thickness. The voltage ratios reach 1.0 for the lowest absorber thicknesses and appear less subject to a decrease for thicker absorbers compared to the current. The logarithmic dependence of current and voltage in the diode equation can serve as an explanation. Interestingly, the FF ratios are close to one for all thicknesses and scatter around this number. While all values given in Figure 1 result from measurements under either 1 sun front or 1 sun rear illumination, it will be insightful to study the performance depending on the level of irradiance as well as under combined front and back illumination.

Aside from the considerations of charge-carrier generation, also the light in-coupling into the solar cell structure plays a major role. Depending on the respective layers above the absorber, substantial differences can occur in the asymmetric thin-film structures. Furthermore, the integration of nanostructures for efficient light management plays an important role, which can help to improve light coupling as well as light localization in ultrathin devices and boost in particular the rear performance^[7] (Annotation: We deliberately choose the term “light localization” rather than “light trapping”. In this way, we aim to avoid a restriction to effects of light redirection toward the horizontal by total internal reflection or waveguide modes. Instead, effects like near-field enhancement or nanojets—for the latter,

see the aforementioned reference—which also lead to field enhancement inside the absorber, shall equally be covered.). Here, we will investigate nanomeshes based on self-assembled sphere patterns, which have the potential for low-cost large-scale fabrication.^[8] At the same time, they offer interesting point contact passivation properties together with a tunability of the nanostructure height to possibly exploit additional morphological and optical effects.

Aside from the assumed perpendicular illumination from the front and the rear side, also the angled light incidence is of interest. This does not only relate to bifacial solar cells, but is relevant for simulating the behavior in a practical environment for any system operated without tracking. The changing irradiance over the day may have a significant impact on the performance of the device and therefore was investigated for mostly silicon solar cells before.^[9] We apply angular-resolved JV measurements as outlined in the norm DIN EN 61853-2 VDE 0126-34-2:2017-05^[10] and by Hermann et al.^[11] to ultrathin CIGSe solar cells without and with nanostructures to depict their performance behavior.

2. Background and Setups

2.1. Bifacial Current–Voltage Characterization

For bifacial JV measurements, different approaches exist, which are defined in the technical specification DIN IEC/TS 60904-1-2 VDE V 0126-4-1-2:2022-04^[3] and are discussed in the following.

The most realistic configuration is to measure under simultaneous front- and rear-side illumination as would be the case in outdoor installations. However, the corresponding setup is not readily available in every lab so alternative and ideally equivalent approaches are sought. Two approaches are covered by the technical specification IEC/TS 60904-1-2 and their equivalence is to be verified for different solar cell technologies. For c-Si, several investigations exist, revealing the exchangeability of the methods^[3,12] and also pointing out challenges during measurements.^[6] For thin-film solar cells, however, the studies are rare so far and mostly come along with investigating specific thin-film topics like buffer variation in BSTUT CIGSe solar cells.^[13]

Before specifying the details of the norm IEC/TS 60904-1-2, we want to pose two major questions to be answered in the beginning for the respective technology (remark: for the sake of simplicity, we will often use 1, 0.1, 0.2 sun, etc. in replacement of 1000, 100, 200 W m⁻², etc.): Q1) What is the solar cell performance under various illumination intensities starting from 0.1–1 sun and potentially beyond? Q2) How does the performance differ between front- and rear-side illumination (only)?

If these points are answered, the subsequent question is the comparability of these (and summed) results to simultaneous front and rear illumination.

Following, we will summarize IEC/TS 60904-1-2 while keeping an eye on aforementioned aspects. The essential feature related to Q1 is the linearity of the J_{sc} with increasing light intensity and the logarithmic following of the V_{oc} according to $V_{oc}(C) = V_{oc}(1) + Ak_B T/q \ln(C)$, where A is the diode quality factor, k_B Boltzman's constant and q the elementary charge. C represents the concentration factor or the illumination intensity in suns, respectively. Depending on the trends of FF influenced mostly by changes in resistances, the efficiency η will follow these trends to a certain extent.

The second question relates to the so-called bifaciality or bifaciality factor, which is essentially defined by the ratio of the respective parameter under rear to front illumination. Specifically, the bifaciality of the J_{sc} is

$$\varphi_{J_{sc}} = \frac{J_{sc, rear}}{J_{sc, front}} \quad (1)$$

Accordingly, the bifaciality of V_{oc} and P_{max} is defined by

$$\varphi_{V_{oc}} = \frac{V_{oc, rear}}{V_{oc, front}} \quad \text{and} \quad \varphi_{P_{max}} = \frac{P_{max, rear}}{P_{max, front}} \quad (2)$$

respectively, and any other parameter may be treated in the same manner.

So far, we have only considered one-sided illumination but under varying illumination intensities and under comparison of front and rear illumination. By doing so, we can address one approach described in the technical specification which enables a bifacial measurement under front illumination only, yet under an equivalent irradiance level G_e . Different fixed rear illumination irradiances G_r , e.g., of 100 and 200 W m⁻², are assumed, which then are not just added to the standard 1000 W m⁻² front illumination but weighted with the bifaciality factor

$$G_e = 1000 \frac{W}{m^2} + \varphi \cdot G_r \quad (3)$$

According to the norm, the minimum of the bifaciality factor of J_{sc} and P_{max} is to be chosen, i.e.

$$\varphi = \min(\varphi_{J_{sc}}, \varphi_{P_{max}}) \quad (4)$$

The practical test, however, pointed to a higher accuracy when using $\varphi_{J_{sc}}$ only and even considering it for the respective G_r (100, 200, etc. W m⁻²) rather than for the case of standard test conditions (1000 W m⁻²).^[5]

Measurements are to be taken for at least two values of G_r and P_{max} plotted against these values (not against G_e). The challenge lies in the fact that G_e is set and measured, while G_r is not but required for the plot.^[6] The linear least squares fitting through the measured points plus forced through the one under standard 1 sun illumination (i.e., $G_r = 0$) is used for extraction of the so-called BiFi factor, which equals the slope and carries the unit of W/(W m⁻²).

In the other, more straightforward configuration, which however requires a bifacial cell tester (BCT) as described later, the solar cell is simultaneously illuminated with 1 sun front and 0, 0.1, or 0.2 sun rear illumination. The plotting of the results against G_r again delivers the BiFi factor. Hereby, the G_r values have been measured directly.^[6] According to the literature, the measured power under simultaneous illumination tends to be smaller than the sum of front plus rear-illuminated power due to series resistance losses. Comparative measurements are especially required when the bifaciality factor is smaller than 1.^[4] As we will find the bifaciality factor for ultrathin CIGSe solar cells to be in the range of 60–80%, we will compare in detail the plots of power against G_r for the two methods of front illumination with compensated irradiance and simultaneous illumination from both sides. Further insight can be obtained by comparing the simple addition of powers, e.g., 1 sun front plus 0.1 or 0.2 sun rear illumination intensity to the results obtained by following the two approaches of the technical specification.

For measurements under a variable illumination intensity from one side, we use a concentrator sun simulator with light source from Photo Emission Tech., Inc. (PET SS5AAA-100 Suns) enabling irradiances up to 100 suns also in combination with glass stack filters for intensity reduction and tuning.^[14] For two-sided illumination, we construct a BCT as initially proposed by Ohtsuka^[15] and Ezquer.^[16] Our specific configuration is depicted in **Figure 2**. The setup is placed under a standard AAA sun simulator from Wacom (WXS-140-SUPER) and the light is routed to the front and the rear side of the perpendicularly mounted solar cell via 45° mirrors. Instead of the mesh used by Ezquer et al. for rear intensity adjustment, we implement neutral density (ND) filters, see later. We ensure the suppression of reflections by enclosing the setup with black-painted metal shields as required in the technical specification. For single-sided measurements, a black curtain is used to block light incidence from the opposite side. Temperature stabilization is challenging underneath our continuous source sun simulator where active cooling is only possible via a fan and the room air-conditioning. The mounting of Peltier elements is not compatible with bifacial

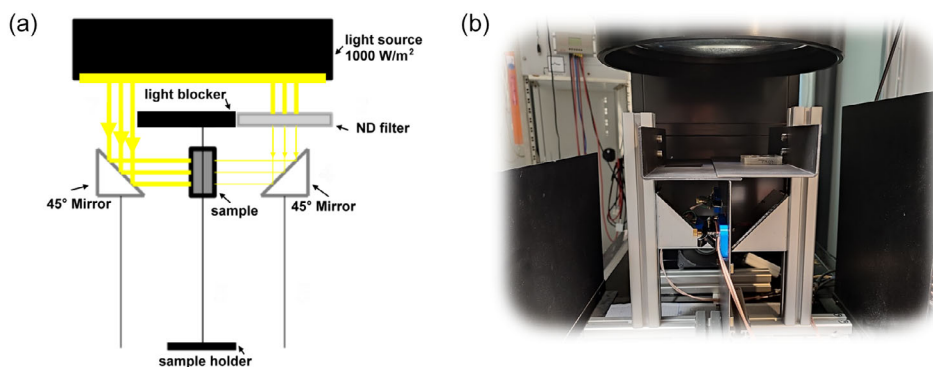


Figure 2. Bifacial cell tester (BCT) for JV measurements under simultaneous front and rear illumination: a) sketch of the setup (adapted with permission) and b) experimental realization.

illumination. Therefore, the degradation behavior of the solar cells can be linked to sample heating.

Asides from this, the filters can be regarded as the most critical component of the BCT setup. Rarely, they provide exactly 0.1 or 0.2 sun transmission. Therefore, we determine the actual precise value by first measuring a silicon reference solar cell under the respective ND filter and then deducing the filter attenuation by assuming linearity in short-circuit current I_{sc} . Importantly, these measurements were performed with the sample mounted in the BCT so that the reflection behavior of the mirror was considered at the same time. The resulting transmission values that were then translated to the irradiance by multiplying with 1000 W m^{-2} are summarized in **Table 1**. These values are considered in the following.

2.2. Angular-Resolved Current–Voltage Characteristics

While the bifacial measurements described earlier consider an illumination under increased light intensity—either from one or two sides—they do not take into account any oblique light incidence. However, in real applications, additional irradiance incident onto bifacial solar cells is exactly expected to emerge from diffuse components of the solar irradiance.

We will address this non-perpendicular incidence of light and investigate the angular-dependent performance of the ultrathin CIGSe solar cells. The technical norm DIN EN 61853-2 VDE 0126-34-2:2017-05^[10] provides the basic details for determining the effect of the angle of light incidence: the angle θ is measured

Table 1. Optical filters used for BCT: transmission from data sheet versus the one calculated from I_{sc} measurements of a Si reference solar cell. The bold parts highlight the important numbers that are used while the rest illustrates the intermediate steps only.

Filter type	OD	I_{sc} [mA]	Transmission [%]	
	Data sheet	Si solar cell	Data sheet	I_{sc} calculated
without	0	2.86	100	100.00
NE203B	0.3	1.38	50	48.22
NE205B	0.5	0.939	32	32.85
NE207B	0.7	0.641	20	22.43
NE210B	1	0.301	10	10.53

from the normal of the solar cell or module and needs to be determined with an accuracy of 1° . The JV measurements are taken in steps of maximum 10° for $\theta \leq 60^\circ$ and in steps of maximum 5° for larger angles. Interestingly, for the sun simulator, class B/C is accepted regarding homogeneity and collimation of the light source, while a temperature measurement (not stability) with an accuracy of 1° is requested. To assure temperature stability, shading of inactive areas and temperature stabilization are required, as well as a potential correction to 25°C . The temperature stabilization is however questionable if continuous light sources are used where we favor fast measurements (≤ 2 s per JV characteristic).

Our angular cell tester (ACT) is depicted in **Figure 3** and it is essentially a rotational stage on which the sample is mounted for JV characterization. Light illumination can take place from either the front or rear side. Despite the restriction to class B/C, particular attention needs to be paid to the illumination homogeneity in the volume traversed by the sample during rotation as also outlined in refs. [9,17]. To minimize variations, we center the sample on the rotational axis and ensure the beam intensity doesn't exceed 1000 W m^{-2} at any point of the cell by measuring the J_{sc} . In our setup, the temperature cannot be controlled for $\pm 1^\circ$. We use a steady-state sun simulator leading to gradual heating, which we attempt to minimize by fast measurements. Reference measurements with thermocouples showed a temperature increase of up to 3°C . Active cooling is only possible via the room air-conditioning and a fan. Since we want to perform measurements from the front and the rear side of the sample, a Peltier element could not be applied. Nevertheless, we will see that the data closely follow the expected trends.

The data can be processed in three steps:^[11] 1) measurement of $J_{sc}(-80^\circ < \theta < 80^\circ)$, 2) normalization of $J_{sc}(\theta)$ to $J_{sc}(0)$ (perpendicular incidence), and 3) division of the latter values by $\cos(\theta)$ to compensate for the enlarged illumination area and thus the reduced light intensity.

Alternatively, we will apply cosine fitting to the J_{sc} curves and reveal how the other solar cell parameters (V_{oc} , FF , η) change as a function of the incidence angle.

Existing literature on the topic is restricted to a basic investigation of the method^[9] and module characterizations identifying limitations of the norm and requesting measurements on cell level.^[11] In particular the variation of incidence angle to be kept

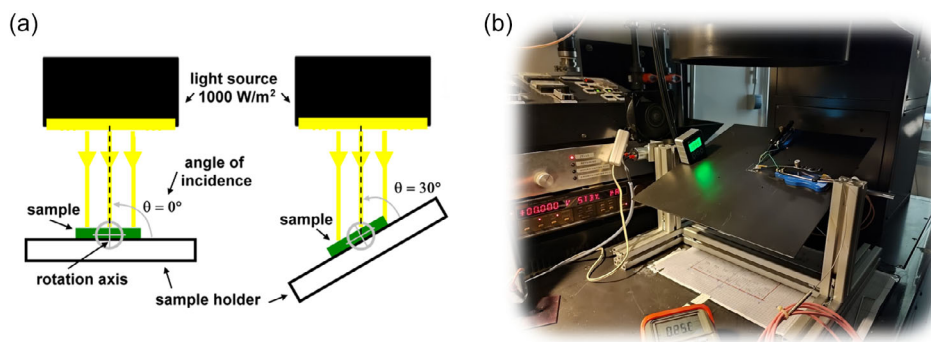


Figure 3. Angular cell tester (ACT) for JV characterization under varying angles of light incidence: a) sketch of the setup and b) experimental realization.

$<1^\circ$ and the volume nonuniformity of irradiance $\leq 2\%$ were highlighted, which are however not an issue in our configuration since we position the solar cell of 0.5 cm^2 size immediately on the rotational axis. Aside, few publications exist on research-oriented questions like the angular-dependent behavior of textured silicon solar cells with and without nanoparticles^[18] or the one of organic tandem solar cells.^[19] Here, we will investigate the angular-resolved performance of ultrathin CIGSe solar cells with integrated nanostructures.

3. Results and Discussion

We start by looking at the characterization results of the ultrathin CIGSe solar cells without and with integrated nanostructures under various illumination conditions. The nanostructures are point contact structures fabricated by nanosphere lithography and deposition of SiO_2 films with different heights (see the experimental section). **Table 2** provides an overview of the solar cell parameters J_{sc} , V_{oc} , FF , and $\eta^* = p_{max}/(1 \text{ sun})$, where p_{max} is the power per solar cell area. Results for illumination with varying intensity from the front only, from the rear only, and from the rear under an additional 1 sun (1000 W m^{-2}) front irradiance are given in Table 2. The odd numbers of variable illumination result from a detailed characterization of filter transmission, see the setups section and Table 1. The performance values relate to the best stable cells of the respective type (0, 25, or 75 nm SiO_2), which mostly show the same trends as the general average over 8 cells (given in Table S1, Supporting Information, whereby it has to be mentioned that these measurements were taken ≈ 1 month before the bifacial test series). An important note is that during the extensive bifacial measurement series with a continuous light source, some cells degraded so that repetitions on fresh cells were performed. As a result, particular trends comparing the performance of 0, 25, or 75 nm SiO_2 may have become more or less pronounced. This was accepted in favor of the best possible comparability of the different bifacial configurations. A supplementary file provides the full-time evolution of the data summarized in Table 2 and beyond. $\eta^* = p_{max}/1 \text{ sun}$ values, i.e. power density measured under various illumination conditions but always normalized to 1000 W m^{-2} , are given here instead of efficiencies for better illustration of the gain. This was done for increased as well as for reduced light intensity, and in particular, later the angular-dependent efficiencies were

also normalized to the 1 sun light incidence despite per actual solar cell area the irradiances are reduced.

Generally, the solar cells with integrated nanostructures show an enhancement in all parameters except for V_{oc} of the 25 nm SiO_2 sample, with the strongest contribution in FF . Only in selected cases (indicated by the grey font in Table 2), usually under simultaneous front and rear illumination, the cells subject to long measurement series reveal a degradation leading to deviations from the general trends. In particular, the solar cells with the thicker (75 nm) SiO_2 deliver the overall best performance (see particularly the boldly highlighted parameters in Table 1). Looking at J_{sc} , under 1 sun front irradiance, we find in Table 2 an increase of $\approx 0.5 \text{ mA cm}^{-2}$ with the addition of SiO_2 . This improved current collection, especially when rear illumination is applied, deserves more detailed studies in the future, where also joint optoelectronic properties of the nanostructures are considered. As the focus of this article is on the bifacial investigation, we do not delve into detail here, but highlight the current enhancement of 2 mA cm^{-2} for the 25 nm SiO_2 sample under 1 sun front and 1 sun rear irradiance.

Regarding V_{oc} , under 1 sun, 25 nm SiO_2 leads to a reduction compared to the case without nanostructures, whereas the 75 nm SiO_2 sample shown here provides an enhancement of $\approx 10 \text{ mV}$ for front and 30 mV for rear illumination (for the average even 50 mV, see Table S1, Supporting Information). This is an interesting observation, which is first in line with our earlier publications that point contact passivation may not be beneficial for CIGSe on transparent conductive back contacts forming a Schottky barrier.^[20,21] Second, the V_{oc} enhancement for the thicker SiO_2 highlights the importance of future consideration of effects arising from nonplanar point-contact structures. It shall be noted that the mentioned changes in J_{sc} and V_{oc} are of an order comparable to measurement errors and statistical variations. Nevertheless, we observed the same trends as described here in similar experimental series presented, e.g., in ref. [22]. Most striking is the significant increase in V_{oc} with SiO_2 under irradiances lower than 1 sun: $\approx 200 \text{ mV}$ are gained under 0.1 sun front and 250 mV under 0.1 sun rear irradiance with the addition of 75 nm SiO_2 (Table 2). This huge rise levels out as the irradiances are increased to 1 sun and beyond.

As mentioned earlier, for the samples represented here, the highest gain is found in FF throughout all illumination conditions. Particularly, it rises by 5% and 11% absolute for 25 and

Table 2. Results of solar cell characterization under various illumination conditions. $\eta^* = p_{\max}/(1 \text{ sun})$ denotes the power density measured under various illumination conditions but always normalized to 1000 W m^{-2} . Best cell results for ultrathin CIGSe solar cells on ITO with 0, 25, and 75 nm high SiO_2 nanostructures are compared. The bold font emphasizes the most important numbers and are highlighte in the text. The grey font refers to data that are expected to be prone to sample degradation as mentioned in the text. The shading colors are providing an important correlation to the colors used for representing the respective samples in the following graphs.

		$J_{sc} [\text{mA cm}^{-2}]$														
Front irradiance [W m^{-2}]		105.3	224.3	328.5	482.2	1000	0	0	0	0	0	1000	1000	1000	1000	1000
Rear irradiance [W m^{-2}]		0	0	0	0	0	105.3	224.3	328.5	482.2	1000	105.3	224.3	328.5	482.2	1000
SiO ₂ thickness	0 nm	2.41	4.90	7.37	11.12	22.39	1.91	3.87	5.80	8.73	17.55	24.20	26.12	28.04	30.96	39.42
	25 nm	2.48	5.01	7.52	11.36	22.86	1.97	3.98	5.95	8.98	18.09	25.27	27.28	29.26	32.30	41.50
	75 nm	2.48	5.00	7.53	11.39	22.79	1.94	3.89	5.87	8.90	17.82	24.99	26.97	28.98	32.05	41.11
		$V_{oc} [\text{mV}]$														
Front irradiance [W m^{-2}]		105.3	224.3	328.5	482.2	1000	0	0	0	0	0	1000	1000	1000	1000	1000
Rear irradiance [W m^{-2}]		0	0	0	0	0	105.3	224.3	328.5	482.2	1000	105.3	224.3	328.5	482.2	1000
SiO ₂ thickness	0 nm	319.1	457.7	520.2	562.6	611.1	236.4	383.1	458.0	514.0	580.0	612.7	616.7	619.6	625.2	632.4
	25 nm	471.5	519.3	540.0	559.6	592.6	441.9	498.3	521.0	542.5	577.9	592.2	595.6	598.5	602.2	612.4
	75 nm	511.2	552.1	572.7	590.9	621.0	490.3	534.7	557.2	578.0	611.8	614.3	618.2	620.9	626.2	637.1
		$FF [\%]$														
Front irradiance [W m^2]		105.3	224.3	328.5	482.2	1000	0	0	0	0	0	1000	1000	1000	1000	1000
Rear irradiance [W m^2]		0	0	0	0	0	105.3	224.3	328.5	482.2	1000	105.3	224.3	328.5	482.2	1000
SiO ₂ thickness	0 nm	31.77	34.18	40.06	45.84	53.34	28.03	31.83	35.69	39.45	46.78	52.40	52.72	52.78	52.77	50.87
	25 nm	45.14	54.56	57.81	59.30	58.23	39.65	48.06	50.46	50.71	49.44	57.16	56.54	55.98	55.22	52.47
	75 nm	54.89	61.06	63.22	64.69	64.77	48.99	53.27	54.04	53.97	52.60	58.86	58.85	58.71	58.58	58.14
		$\eta^* [\%]$														
Front irradiance [W m^{-2}]		105.3	224.3	328.5	482.2	1000	0	0	0	0	0	1000	1000	1000	1000	1000
Rear irradiance [W m^{-2}]		0	0	0	0	0	105.3	224.3	328.5	482.2	1000	105.3	224.3	328.5	482.2	1000
SiO ₂ thickness	0 nm	0.24	0.77	1.53	2.87	7.30	0.13	0.47	0.95	1.77	4.76	7.77	8.49	9.17	10.22	12.68
	25 nm	0.53	1.42	2.35	3.77	7.89	0.35	0.95	1.56	2.47	5.17	8.55	9.18	9.80	10.74	13.34
	75 nm	0.70	1.69	2.73	4.35	9.17	0.46	1.11	1.77	2.78	5.74	9.04	9.81	10.57	11.76	15.23

75 nm SiO_2 , respectively, under 1 sun (Table 2). In the end, the highest power density per 1 sun is reached by the sample with 75 nm SiO_2 : 9.17% under 1 sun front illumination, 9.81% with an added 0.2 sun rear irradiance as the norm specifies, and finally 15.23% under 1 sun from the front plus 1 sun from the rear. In conclusion, the integration of SiO_2 nanostructures as well as the bifacial operation lead to a considerable power enhancement of the ultrathin CIGSe solar cells on indium tin oxide (ITO).

The changes in measured solar cell parameters can well be brought in line with results from a one-diode fitting of the respective JV curves. Table 3 juxtaposes J_{sc} , V_{oc} , FF , and η as given in Table 2 to the fitted diode parameters shunt resistance R_{sh} , series resistance R_s , diode quality factor A , and dark saturation current density J_0 . The increasing FF s with thicker SiO_2 are directly correlated with higher shunt resistances; this is equally true for the comparison of front versus rear illumination, where the lower values for the latter case align. The series resistances reveal a correlation with the V_{oc} whereby a higher V_{oc} is linked with a lower R_s and a minimum of 1.58 Wcm^2 is reached for the highest V_{oc} .

Table 3. Solar cell parameters for ultrathin CIGSe solar cells on ITO with 0, 25, and 75 nm high SiO_2 nanostructures juxtaposed to results from one-diode fitting delivering shunt resistance R_{sh} , series resistance R_s , diode quality factor A , and dark saturation current density J_0 . (1,0) denotes 1 sun front, (0,1) denotes 1 sun rear illumination.

	0 nm SiO_2		25 nm SiO_2		75 nm SiO_2	
	(1,0)	(0,1)	(1,0)	(0,1)	(1,0)	(0,1)
$J_{sc} [\text{mA cm}^{-2}]$	22.39	17.55	22.86	18.09	22.79	17.82
$V_{oc} [\text{mV}]$	612.8	580.0	592.6	577.9	621.0	611.8
$FF [\%]$	54.16	46.80	58.36	49.44	64.80	52.72
$\eta [\%]$	7.43	4.76	7.91	5.17	9.17	5.75
$R_{sh,diode} [\Omega\text{cm}^2]$	112.47	84.48	258.48	149.04	668.36	231.22
$R_{s,diode} [\Omega\text{cm}^2]$	2.23	2.89	2.71	5.94	1.58	5.29
A	2.16	2.44	2.11	2.36	2.23	2.48
$J_0 [\text{mA cm}^{-2}]$	2.64 E-04	0.001	3.57 E-04	0.001	3.94 E-04	0.001

The diode quality factor shows the largest difference between front and rear irradiance rather than between different SiO₂ thicknesses. This observation confirms that the lower-quality diode under rear condition is characterized by a higher A. The same is true for J₀ with approximately one order of magnitude larger values for rear irradiance. In summary, the diode fits confirm the reduced performance under rear illumination and the improvement with 75 nm SiO₂ nanostructure integration.

The previous discussion was mostly devoted to the performance comparison of the here-introduced samples of ultrathin CIGSe solar cells without and with integrated SiO₂ nanostructures. It was revealed, that the nanostructures can have various influences including related optical and electrical properties. As will be highlighted at the end of the discussion on bifacial properties, also structural and compositional influences may play a role. Altogether, these aspects deserve further study and cannot be entirely resolved here. We continue on the core focus of the manuscript which is the investigation of CIGSe solar cell behavior under different light intensity levels and the determination of the bifacial performance. Importantly, we will compare the two measurement approaches outlined in the background section. **Figure 4a** starts by showing the evolution of the J_{sc} as a function of irradiance from either front or rear side. The data were measured using the BCT and thus provide values close to 0.1, 0.2, 0.3, 0.5, and 1 sun. As mentioned earlier, the differences in current

between the different SiO₂ thicknesses are small with a trend to higher values for the nanostructure-containing ones. The expected linearity of current with irradiance is well fulfilled as the lines for a guide of the eye underline. The linearity beyond 1 sun was additionally tested using the concentrator sun simulator and can also be regarded as mostly fulfilled. Figure S1a depicts the according data and the line there is the extrapolation of J_{sc} = 22.35 mA cm⁻², being the average J_{sc} at 1 sun for the three types of cells, to other irradiances. The variations above 1.5 suns are larger than below 1 sun and a trend toward an over-estimation of current in this setup is observed for the high irradiances (which are however not part of the norm). The dense data points between 1 and 1.5 suns are the results of testing different G_e (see the discussion later) and the variations in J_{sc} for closely neighboring irradiances underline the later-made statement of comparability within the error margin.

Beyond the linearity in current, the information in Figure 4a that brings us further in the bifacial cell testing is the difference in performance under front and rear illumination. The lower values obtained for the latter case deliver bifaciality factors smaller than one, which amount to ≈80% in J_{sc} for all SiO₂ thicknesses and irradiances as represented in Figure 4b by the solid points. The lower performance under rear illumination can be linked to a worse separation of carriers generated further from the space-charge region.^[23] Additionally, we depict the bifaciality factor of

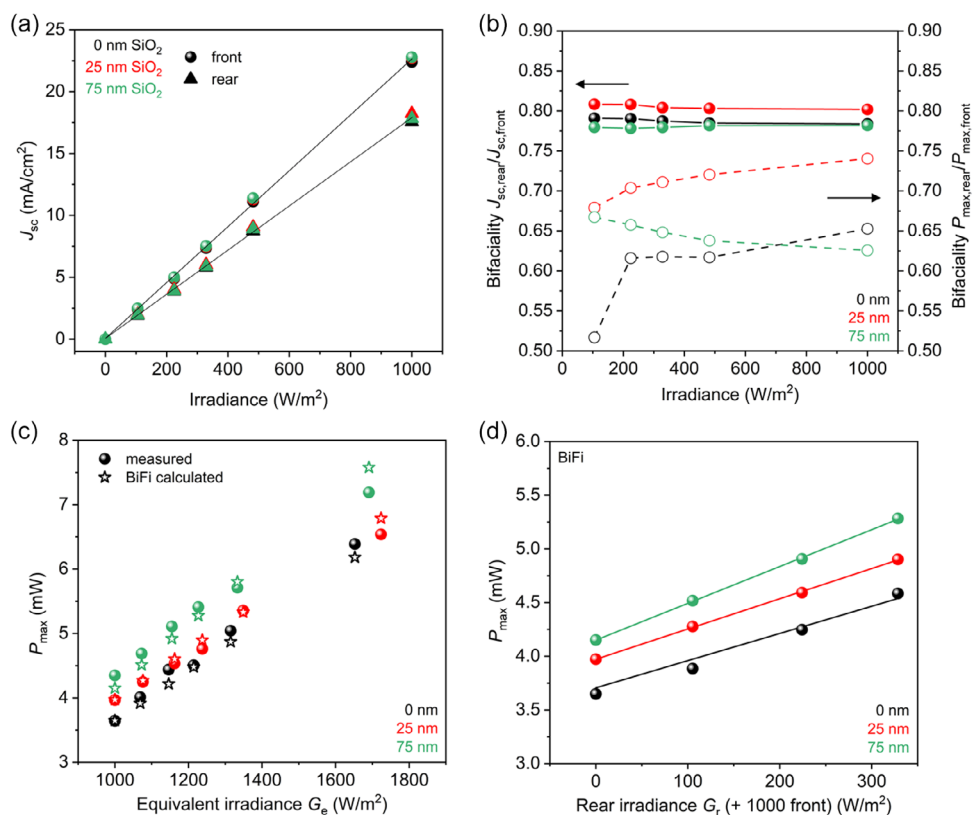


Figure 4. Bifacial performance evaluation of ultrathin CIGSe solar cells on ITO with 0, 25, and 75 nm high SiO₂ nanostructures. a) Front and rear short-circuit current density as a function of irradiance below 1 sun and b) resulting bifaciality factor of J_{sc} (solid) and additionally of maximum power (open/dashed); c) P_{max} measured under equivalent irradiance as calculated based on bifaciality of power in comparison to values calculated from the d) BiFi fit on bifacial power measurements.

maximum power by open circles, showing lower values than for the current with on average 65%. The norm specifies that the minimum of the bifaciality factor of J_{sc} and P_{max} is to be chosen, so we are left with the one for the power.

The increased irradiance from the front, which is equivalent to bifacial illumination, can then be calculated by reducing the rear irradiance according to the bifaciality factor and adding it to the front irradiance. The resulting measurements, using our concentrator sun simulator to generate these equivalent irradiances, are shown by the solid circles in Figure 4c. They are compared to values arising from the BiFi derivation shown in Figure 4d: the maximum power under *BIFACIAL OPERATION* is plotted as a function of *REAR IRRADIANCE* and the linear fit forced through the value of 1 sun front and 0 sun rear. Now, instead of the measurement data for the respective bifacial illumination cases, the corresponding points on the fitting lines are used for comparison to the results of equivalent irradiance in Figure 4c and are depicted as stars. Slight variations are observed, but overall, a very good agreement between the two data sets is given.

Let us come back to the proposal of Rauer et al. to use the $\varphi_{J_{sc}}$ values at the respective G_r instead of $\min(\varphi_{J_{sc}}, \varphi_{P_{max}})$ at 1 sun to calculate G_e .^[5] When doing so, despite the difference in bifaciality factor of J_{sc} and P_{max} being non-negligible, the results in measured power under the slightly different G_e values remain within the error margin of the measurement data obtained according to the norm. Altogether, these results underline that for ultrathin CIGSe solar cells, also with integrated nanostructures, the two measurement approaches defined in the norm for bifacial performance investigation deliver highly comparable results and

can thus both be applied. Notable deviations are only observed under 1 sun front plus 1 sun rear illumination, where non-negligible heating occurs resulting in V_{oc} and FF losses. These high irradiances are however not part of the bifacial cell testing norm, which talks about 1 sun front plus 0.1 or 0.2 sun rear irradiance. In this latter range, the correspondence between the two approaches is very well fulfilled.

In the background part, we concluded the questions with the one about the comparability of front and rear performance and of summed results to simultaneous front and rear illumination. Whereas the first point is essentially answered by the bifaciality factor, **Figure 5** is devoted to the second part. For this purpose, we look into the parameters measured under various sets of front and rear illumination given as *parameter* (“front sun”, “rear sun”) and their addition. Hereby, n is the variable irradiance given on the x axis; it shall be noted that based on the parameters depicted, the value of 1000 W m^{-2} on the x -axis corresponds to a total irradiance of 2 suns in Figure 5a,b,d,e.

For 0 nm SiO_2 , i.e., without nanostructures, in addition to 1 sun front plus n sun rear, the inverse cases of 1 sun rear plus n sun front were measured, whereas this was omitted for the other samples given the observed degradation with multiple recontacting and remeasuring. Starting from the J_{sc} presented in Figure 5a, we find that summing the value measured under 1 sun front ($J_{sc}(1,0)$) and the ones of n sun rear ($J_{sc}(0,n)$) equals the measurement values of simultaneous 1 sun front plus n sun rear irradiance ($J_{sc}(1,n)$). This equally holds for $J_{sc}(n,1) = J_{sc}(n,0) + J_{sc}(0,1)$ with a perfect match. The absolute lower values of $J_{sc}(n,1)$ compared to $J_{sc}(1,n)$ are the result of the generally observed lower rear performance. For $J_{sc}(1,1)$,

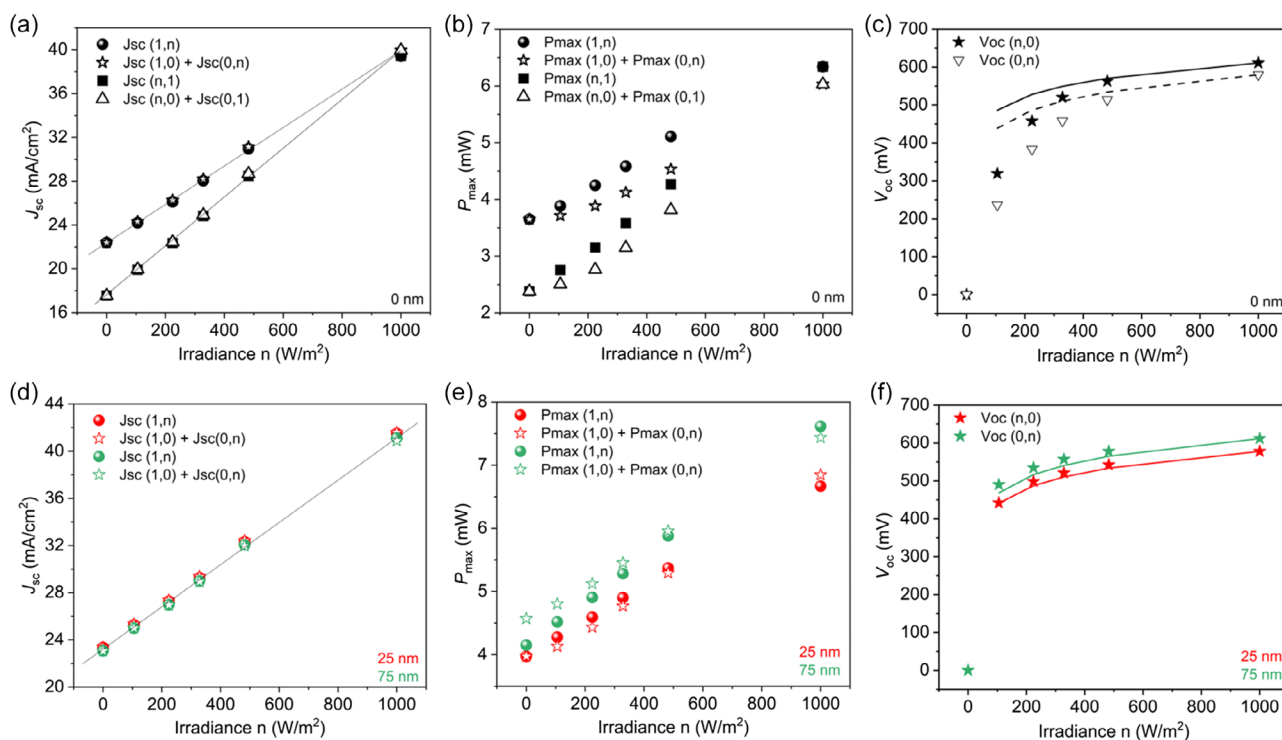


Figure 5. Summation of front plus rear performance in comparison to bifacially measured results. a–c) J_{sc} , P_{max} , and V_{oc} comparison for the ultrathin CIGSe on ITO without nanostructures; d–f) analog for the samples with 25 or 75 high SiO_2 nanostructures.

the values coincide again as the front and rear performances contribute with equal weight.

Looking at the maximum power (Figure 5b), we however observe deviations between front performance under 1 sun plus rear performance under n sun compared to the values under corresponding bifacial illumination and equally for $P_{\max}(n,1)$ compared to $P_{\max}(n,0)+P_{\max}(0,1)$. A deviation was to be expected, otherwise bifacial measurements would not be required. Yet, given the perfect match of summed and bifacially measured J_{sc} , the results may appear surprising. What is the reason? The behavior may be explained by the fact that bifacial operation corresponds to operation under light concentration. The larger the total illumination intensity, the higher the performance increase compared to 1 sun irradiance. The expected logarithmic behavior of V_{oc} for >1 sun irradiance is well fulfilled—even within the error range of repeated measurements using the concentrator sun simulator (Figure S1b, Supporting Information). The absolute V_{oc} increase from 1 to 1.5 sun, however, is only 23 mV, so that the strong rise in power appears surprising, in particular as literature suspects reduced performance due to increased resistance losses.^[4] The answer for our observed behavior is rather found in the V_{oc} behavior below 1 sun. Figure 5c shows the related front- and rear-sided V_{oc} dependence. The lines represent the V_{oc} extrapolation from $V_{oc}(1)$ according to $V_{oc}(n) = V_{oc}(1) + Ak_B T/q \cdot \ln(n/1000)$, where A is the diode quality factor from Table 2 and $k_B T/q = 25.69$ mV the thermal voltage. A significantly stronger drop as expected is observed for the experimental values, particularly under rear irradiance. This is in line with the very low shunt resistances found for the sample without SiO_2 which can be associated with poor low-light performance.^[24] Thus, the V_{oc} contribution falling back under low irradiance leads to significantly lower values of summed single-sided power results compared to bifacial measurements.

In Figure 5d–f, the previously outlined comparison of summed and bifacial results, now considering only 1 sun front and n sun rear irradiance, is given for the samples with 25 or 75 nm SiO_2 . As for the samples without nanostructures, the match of $J_{sc}(1,n)$ with $J_{sc}(1,0) + J_{sc}(0,n)$ is perfect (Figure 5d). Deviations of $P_{\max}(1,n)$ from $P_{\max}(1,0)+P_{\max}(0,n)$ are smaller than for the case without nanostructures (Figure 5e compared to Figure 5b). It has to be noted that for these comparisons, we use the parameter values of 1 sun irradiance measured in the same series to stay most comparable. With integrated SiO_2 , the performance of V_{oc} at low irradiances follows well the expected logarithmic trend (Figure 5f), supporting the close correspondence of the summed and the bifacially measured power values. Apparently, for the ultrathin CIGSe solar cells on ITO with integrated nanostructures, the performance under increased irradiance from bifacial illumination does not noticeably surpass the summed front and rear performance as a stable low-light-intensity behavior is achieved.

Altogether, we note that the integration of SiO_2 nanostructures can support performance stability at low-light irradiance. Along with higher V_{oc} values for the 75 nm SiO_2 samples, we find indications that the integration of ELEVATED dielectric nanostructures in ultrathin CIGSe solar cells is beneficial even on ITO. While the bare effect of point contact passivation on transparent conductive back contact can be seen skeptically,^[20,21]

additional structural and electrical effects arising from nonplanar nanostructures should not be overlooked. Two aspects shall be highlighted here: first, the elevated nanomeshes can foster In–Ga interdiffusion, leading to a higher minimum bandgap in the Ga gradient and thus increasing V_{oc} .^[8] Second, a potential GaO_x formation (aspired to be suppressed additionally by starting the CIGSe deposition with indium—see Section 5 and ref. [25]) is expected to be moved toward the bulk. The oxygen provided for GaO_x formation during CIGSe growth is only available at the non-passivated ITO back contact or from the SiO_2 nanomeshes. The latter is however further from the back contact, thus shifting also trap states related to GaO_x toward the bulk. The reduction of recombination centers and trap states at the rear interface can be linked to an increased lifetime and a higher recombination resistance, associated with a higher V_{oc} . Closely related is an effective extraction of charge carriers contributing to a stable J_{sc} . Further tuning of the nanostructure shape and height is expected to reveal a sweet spot for structural, electrical, and also optical performance optimization and deserves special attention and comprehensive investigations in future research of BSTUT CIGSe solar cells.

Given the previous discussion, we focus on samples with 75 nm SiO_2 to perform the angular-dependent JV characterization. For minimizing the effects arising from sample stress due to extensive measurement series, we use a separate set of samples. Therefore, the exact values are not the same as in the previous figures and tables θ , but what we research here are the trends as a function of light incidence angle θ . Figure 6 depicts J_{sc} , V_{oc} , FF , and η under front (bubbles) and rear (triangles) irradiance whereby θ is varied between $+70^\circ$ and -70° . Accordingly to the bifacial measurements, we present an angular efficiency here which results from the maximum power normalized to 1000 W m^{-2} for all cases despite the irradiance changes with the angle.

The norm and Hermann et al.^[11] describe the normalization of $J_{sc}(\theta)$ with $J_{sc}(0)$ followed by the division with $\cos(\theta)$ to obtain a line. We perform the alternative approach of showing the measurement data directly and fitting them with $J_{sc}(0) \cdot \cos(\theta)$. In this way, we stay consistent with the later discussion of other parameters. As Figure 6a reveals, the J_{sc} very well follows the expected cosine behavior. A small asymmetry in the data leading to slightly higher values at positive angles results from sample heating during the measurement series taken from $+70^\circ$ to -70° and is not a result of a possible asymmetry of the setup. No strong rise of current values beyond the cosine curve for larger angles underlines that these 75 nm SiO_2 nanomeshes do not yet show strong optical effects, leaving room for further optimization of optoelectronic properties in the future.

Looking at V_{oc} (Figure 6b), we also find the expected angular-dependent behavior with fitting curves extrapolated from 0° that can represent the data within the error margin. For the fits, we again chose the logarithmic dependence on light intensity and an according reduction given by $V_{oc}(\theta) = V_{oc}(0) + Ak_B T/q \cdot \ln(\cos(\theta))$, with A the respective diode factors of this sample. The FF depicted in Figure 6c remains almost constant over an angular range from $+35^\circ$ to -35° and then starts to drop more slowly than V_{oc} . A flatter behavior is in line with the FF following V_{oc} in an attenuated way (for formulas, see^[26]). Given the minor angular dependence of FF , the

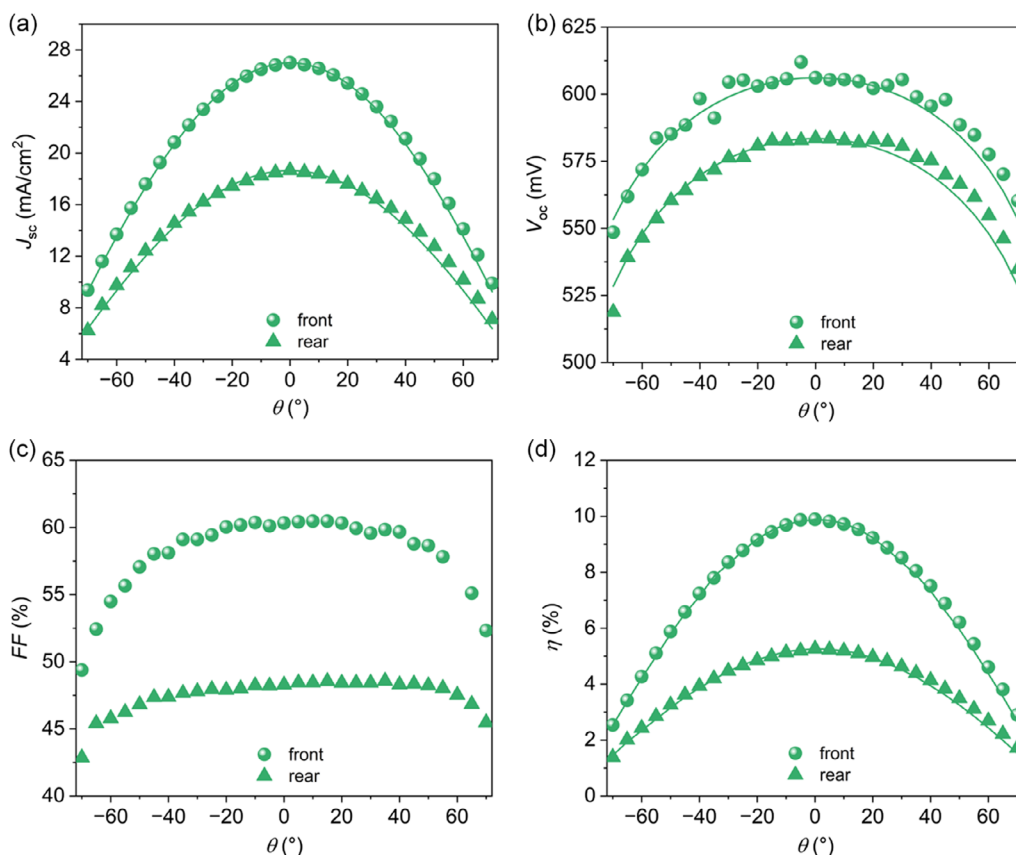


Figure 6. Angular-dependent JV performance of bifacial semitransparent ultrathin CIGSe solar cells on ITO with integrated 75 nm high SiO₂ nanostructures. a) Short-circuit current density, b) open-circuit voltage, c) fill factor, and d) angular efficiency as a function of light incidence angle θ under front and rear irradiance.

efficiency essentially reflects the changes in J_{sc} and V_{oc} (see Figure 6d with fitting lines based on the fitted V_{oc} and J_{sc}). In summary, the ultrathin CIGSe solar cells on ITO back contact (also with integrated nanomeshes) follow well the expected cosine behavior under angular-dependent irradiance. All these observations are equally true for front and rear illumination.

4. Conclusion

In summary, we have investigated ultrathin CIGSe solar cells on ITO, also with integrated nanostructures, for their bifacial and angular-dependent performance. We find bifaciality factors, i.e., rear over front performance, of $\approx 80\%$ for J_{sc} and of $\approx 65\%$ for maximum power. The bifacial measurement approach of calculating an equivalent front irradiance based on this bifaciality delivers results highly comparable to immediate bifacial illumination. Aside from the standard test conditions of 0.1 and 0.2 sun rear irradiance, also intensities up to 1 sun front and rear were investigated. A degradation of the samples with higher illumination intensities and in particular repetitive measurements was observed, which can be correlated with sample heating. A flash sun simulator would be beneficial, but even under continuous illumination, we find useful results when performing fast measurements and allowing the samples recovery time. Importantly, degradation could

partially be mitigated with the integration of nanostructures. For these, we chose SiO₂ nanomeshes with 25 and 75 nm height and found in particular performance enhancement for the elevated structures. The maximum bifacial efficiency we measured then was 15.23% under 1 sun from the front plus 1 sun from the rear. With integrated nanostructures, even the summation of individual front and rear performance measurements delivered results similar to the bifacial data. Furthermore, the angular-resolved JV characterization performed on the samples with 75 nm SiO₂ very well revealed the expected cosine behavior resulting from the changed irradiation density. Altogether, the procedures for bifacial and angular-dependent performance testing are applicable to BSTUT CIGSe solar cells and integrated nanostructures show benefits for performance enhancement and stabilization.

5. Experimental Section

The samples used were BSTUT CIGSe solar cells consisting of the following layers: 2 mm thick, $2.5 \times 2.5 \text{ cm}^2$ glass substrate, 300 nm TCO layer made from sputtered In₂O₃:Sn (ITO), 475 nm CIGSe grown by co-evaporation of the elements in a three-stage process with a short initial indium supply,^[25] 40 nm chemical bath-deposited CdS, radio frequency (RF)-sputtered i-ZnO and ZnO:Al with 80 and 300 nm thickness, respectively, as well as 10/2000 nm Ni/Al front grids. For the samples including nanostructures at the ITO/CIGSe interface, nanosphere lithography was applied using 1200 nm diameter polystyrene (PS) spheres.

The self-assembled hexagonal sphere pattern was plasma-etched in air atmosphere for 20 min to obtain a template of 900 diameter spheres while keeping the pitch given by the initial diameter.^[21] Subsequently, SiO₂ with a thickness of 25 or 75 nm was evaporated on top of the PS sphere pattern. After lifting off the spheres, a point contact structure remained with the given SiO₂ layer thickness. A similar process is described along with the illustration of further details in ref. [8].

Supporting Information

Supporting Information is available from the Wiley Online Library or from the author.

Acknowledgements

The authors acknowledge J. Kruij for initial experiments with the BCT and ACT setups, J. Lucaßen for discussion, and T.-H. Witte-Nguy for formatting. The authors also acknowledge the support from the Open Access Publication Fund of the University of Duisburg-Essen. [Correction added on 24 October 2024, after first online publication: three formulas in the section 3 (Results and Discussion) have been updated in this version.]

Open Access funding enabled and organized by Projekt DEAL.

Conflict of Interest

The authors declare no conflict of interest.

Author Contributions

Tristan Koehler: Data curation (lead); Formal analysis (equal); Investigation (lead); Methodology (lead); Validation (lead); Visualization (lead); Writing—review and editing (supporting). **Yao Gao:** Data curation (supporting); Formal analysis (supporting); Investigation (supporting); Methodology (supporting); Validation (supporting); Writing—review and editing (supporting). **Martina Schmid:** Formal analysis (equal); Investigation (supporting); Methodology (supporting); Validation (equal); Visualization (supporting); Writing—original draft (lead); Writing—review and editing (lead).

Data Availability Statement

The data that support the findings of this study are available from the corresponding author upon reasonable request.

Keywords

angular-dependent solar cell characterizations, bifacial solar cell testings, semitransparent ultrathin CIGSe solar cells, SiO₂ nanomeshes

Received: June 6, 2024

Revised: August 6, 2024

Published online: September 24, 2024

[1] M. Fischer, M. Woodhouse, P. Baliozian, J. Trube, *International Technology Roadmap for Photovoltaic (ITRPV)*, VDMA, Frankfurt am Main **2023**.

[2] Y. Li, G. Yin, M. Schmid, *Sol. Energy Mat. Sol. Cells* **2022**, 234, 111431.

[3] Norm DIN IEC/TS 60904-1-2 VDE V 0126-4-1-2:2022-04, VDE-Verlag **2019**, <https://www.vde-verlag.de/iec-normen/247146/iec-ts-60904-1-2-2019.html>.

- [4] A. Schmid, G. Dülger, G. Baraah, U. Kräling, F. Ise, in *Proc. 33rd EU-PVSEC Amsterdam*, WIP-Verlag **2017**.
- [5] M. Rauer, A. Schmid, F. Guo, F. Neuberger, P. Gebhardt, J. Hohl-Ebinger, in *Proc. 37th EU-PVSEC, Virtual*, WIP-Verlag **2020**.
- [6] G. Koutsourakis, M. Rauer, A. Schmid, G. Bellenda, T. Betts, J. Blakesley, M. Bliss, J. Bonilla, K. Bothe, S. Dittmann, J. Lopez-Garcia, W. Herrmann, D. Hinken, R. Kenny, R. Molinero, D. Pavanello, S. Riechelmann, H. Sträter, A. Vegas, S. Winter, in *Proc. 37th EU-PVSEC*, WIP-Verlag **2020**.
- [7] a) A. Mavlonov, J. Chantana, T. Nishimura, Y. Kawano, M. Inoue, N. Hamada, T. Masuda, T. Minemoto, *Sol. Energy* **2020**, 211, 725; b) A. Mavlonov, T. Nishimura, J. Chantana, Y. Kawano, T. Masuda, T. Minemoto, *Sol. Energy* **2020**, 211, 1331; c) A. Mavlonov, T. Nishimura, J. Chantana, Y. Kawano, T. Minemoto, *Appl. Phys. Lett.* **2021**, 219, 103903; d) T. Nishimura, N. Hamada, J. Chantana, A. Mavlonov, Y. Kawano, T. Masuda, T. Minemoto, *ACS Appl. Energy Mater.* **2020**, 3, 9504; e) S.-C. Yang, T.-Y. Lin, M. Ochoa, H. Lai, R. K. Kothandaraman, F. Fu, A. N. Tiwari, R. Carron, *Nat. Energy* **2022**, 8, 40; f) M. Mazzer, S. Rampino, G. Spaggiari, F. Annoni, D. Bersani, F. Bissoli, M. Bronzoni, M. Calicchio, E. Gombia, A. Kingma, F. Pattini, E. Gilioli, *Sol. Energy Mat. Sol. Cells* **2017**, 166, 247; g) T. Nakada, Y. Hirabayashi, T. Tokado, D. Ohmori, T. Mise, *Sol. Energy* **2004**, 77, 739; h) D. Kim, S. S. Shin, Y. Jo, S. M. Lee, S. K. Ahn, J.-S. Cho, J. H. Yun, J. H. Park, *Adv. Sci.* **2022**, 9, 2105436; i) D. Kim, S. S. Shin, S. M. Lee, J.-S. Cho, J. H. Yun, H. S. Lee, J. H. Park, *Adv. Funct. Mater.* **2020**, 30, 2001775; j) Y. Li, G. Yin, M. Schmid, *Sol. Energy Mat. Sol. Cells* **2022**, 234, 111431; k) Y. Li, S. W. Tabernig, G. Yin, A. Polman, M. Schmid, *Sol. RRL* **2022**, 6, 2200695; l) M. J. Shin, A. Lee, A. Cho, K. Kim, S. K. Ahn, J. H. Park, J. Yoo, J. H. Yun, J. Gwak, D. Shin, I. Jeong, J.-S. Cho, *Nano Energy* **2021**, 82, 105729; m) M. J. Shin, A. Lee, J. H. Park, A. Cho, S. K. Ahn, D. Shin, J. Gwak, J. H. Yun, J. Yoo, J.-S. Cho, *Nano Energy* **2022**, 92, 106711; n) K. Kim, W. N. Shafarman, *Nano Energy* **2016**, 30, 488.
- [8] G. Yin, M. Song, S. Duan, P. Manley, D. Greiner, C. A. Kaufmann, M. Schmid, *ACS Appl. Mater. Interfaces* **2016**, 8, 31646.
- [9] S. Winter, D. Friedrich, T. Gerloff, in *Proc. 25th EU-PVSEC Valencia*, WIP-Verlag **2010**.
- [10] Norm DIN EN 61853-2 VDE 0126-34-2:2017-05, VDE-Verlag **2017**.
- [11] W. Hermann, M. Schweiger, L. Rimmelspacher, in *Proc. 29th EU-PVSEC Amsterdam*, WIP-Verlag **2014**.
- [12] M. Rauer, F. Guo, J. Hohl-Ebinger, in *Proc. 36th EU-PVSEC Marseille*, WIP-Verlag **2019**.
- [13] D. Kim, S. S. Shin, Y. Jo, S. M. Lee, S. K. Ahn, J.-S. Cho, J. H. Yun, H. S. Lee, J. H. Park, *Adv. Sci.* **2022**, 9, 2105436.
- [14] K. M. Czajkowski, M. Schmid, *IEEE Photonics J.* **2017**, 9, 1.
- [15] H. Ohtsuka, M. Sakamoto, M. Koyama, K. Tsutsui, T. Uematsu, Y. Yazawa, *Prog. Photovolt.: Res. Appl.* **2001**, 9, 1.
- [16] M. P. Ezquer, I. Petrina, J. M. Cuadra, A. R. Lagunas, in *Proc. 23rd EU-PVSEC 2008*.
- [17] J. Kruij, *Bachelor Thesis*, University of Duisburg-Essen **2021**.
- [18] W.-J. Ho, J.-C. Lin, J.-J. Liu, C.-W. Yeh, H.-J. Syu, C.-F. Lin, *Materials* **2017**, 10, 737.
- [19] A. Mertens, J. Mescher, D. Bahro, M. Koppitz, A. Colsmann, *Opt. Express* **2016**, 24, A898.
- [20] Y. Tu, Y. Li, R. Klenk, G. Yin, M. Schmid, *Prog. Photovolt.: Res. Appl.* **2022**, 30, 393.
- [21] Y. Li, G. Yin, Y. Tu, S. Sedaghat, Y. Gao, M. Schmid, *ACS Appl. Energy Mater.* **2022**, 5, 7956.
- [22] T. Koehler, J. Kruij, Y. Gao, J. Lucaßen, Y. Li, M. Schmid, in *2018 IEEE 7th World Conf. Photovoltaic Energy Convers. (WCPEC)*, IEEE, Waikoloa **2023**.

- [23] T. Nishimura, J. Chantana, A. Mavlonov, Y. Kawano, T. Masuda, T. Minemoto, *Sol. Energy* **2021**, 218, 76.
- [24] S. Ishizuka, Y. Kamikawa, J. Nishinaga, *NPJ Flexible Electron.* **2022**, 6, 90.
- [25] C. Rath, Y. Gao, T. Koehler, M. Schmid, *Adv. Mater. Interf.* **2024**, 11, 2400085.
- [26] C. Honsberg, S. Bowden, *PVCDROM - Fill Factor*, pveducation.org/pvcdrom/solar-cell-operation/fill-factor, accessed: April, 2024.

DuEPublico

Duisburg-Essen Publications online

UNIVERSITÄT
DUISBURG
ESSEN

Offen im Denken

ub | universitäts
bibliothek

This text is made available via DuEPublico, the institutional repository of the University of Duisburg-Essen. This version may eventually differ from another version distributed by a commercial publisher.

DOI: 10.1002/aesr.202400168

URN: urn:nbn:de:hbz:465-20251120-091435-7



This work may be used under a Creative Commons Attribution 4.0 License (CC BY 4.0).